CRS4-TECH-REP-02/3

Optimisation of the Pin Cooler design for the Megapie Target using full 3D numerical simulations

S. Buono, L. Maciocco, V. Moreau, L. Sorrentino

CRS4, Centre for Advanced Studies, Research and Development in Sardinia

January 18th 2002

Abstract

The MEGAwatt PIlot Experiment (MEGAPIE) project has been recently proposed to demonstrate the feasibility of a liquid lead bismuth target for spallation facilities at a beam power level of 1 MW. The target will be put into operation at the Paul Scherrer Institut (PSI, Switzerland) in 2004 and will be used in the existing target block of SINQ. About 650 kW of thermal power has to be removed through a bunch of 12 pin-coolers. In order to improve the heat exchange, it was decided to investigate the possibility of accelerating the oil coolant by introducing a spiral in the oil cylindrical channel. This forces the flow to rotate while rising, thus increasing the Reynolds number and the heat transfer coefficient. We show some numerical simulations, which have supported the dimensioning of the pins as well as the choice of the secondary coolant, that is Diphyl THT. The spiral option has been confirmed.

The spiral diameter must be a little smaller than the channel width, to allow the effective mechanical assemblage of the pin. The existence of a gap between the spiral and the external wall adds complexity to the numerical simulation, being fully 3D with several orders of magnitude of length scales involved.

A single pin has been tested by Enea-Brasimone and entirely simulated by CRS4 for a matrix of various operational settings. Results are shown and compared.

Contents

1 Introduction 2
2 Geometrical Description 2
3 Pin dimensioning 4
4 Spiral analysis 5
4.1 From 2D to 3D analysis 5
4.2 Spiral 3D preliminary study 6
4.3 Computational Model 7
4.4 Results 9
4.5 Conclusion 10
5 Pin-cooler 3D numerical simulation 11
5.1 Computational model 11
5.2 Calculation strategy 17
5.3 Results 18
5.4 Discussion 24
6 Conclusions 25
7 References 25

1 Introduction

The MEGAwatt PIlot Experiment (MEGAPIE) project has been recently proposed to demonstrate, the feasibility of a liquid lead bismuth target for spallation facilities at a beam power level of 1 MW The target will be put into operation at the Paul Scherrer Institut (PSI, Switzerland) in 2004 and will be used in the existing target block of SINQ. About 650 kW of thermal power has to be removed through a bunch of 12 pin-coolers. It has been decided to investigate the possibility of accelerating the oil coolant, to improve the heat exchange, by means of the introduction of a spiral in the oil cylindrical channel. This should force the flow to rotate while rising, thus increasing the Reynolds number and the heat transfer coefficient.

Two organic oils were candidates as secondary coolant. The first, Dowtherm A oil, has better heat transfer properties. The second, Diphyl THT oil, has a better behaviour under irradiation. We show, my means of numerical simulations that it is possible to use the second one, provided that the oil channel is made smaller and a spiral is inserted.

The next step was to test a single pin, which has been made in an Enea-Brasimone facility, and to make a numerical simulation at CRS4. The spiral must be a little smaller than the channel width, to allow the effective mechanical assemblage of the pin. The existence of a gap between the spiral and the external wall makes the numerical simulation much more complex, being fully 3D with several magnitude orders between the phenomena to be captured.

We describe the final numerical model and the results obtained which are compared with the experimental measures.

2 Geometrical Description

The pin-cooler is essentially made of 3 concentric annular flows separated by steel walls. The external one is the downcoming PbBi eutectic flow. The intermediate one is the rising oil flow, connected at the bottom to the internal downcoming oil flow. The working height of the apparatus is bounded by the available space and is about 1.3 m. A sketch of the geometry is shown in Figure 1.

A 2D numerical simulation has been done to test this basic geometry in nominal operating conditions, namely with 1/3 l of PbBi entering at 370 ^{o}C and 5/6 l of oil entering at 100^{o}C. Resulting temperatures are shown in Figure 2.

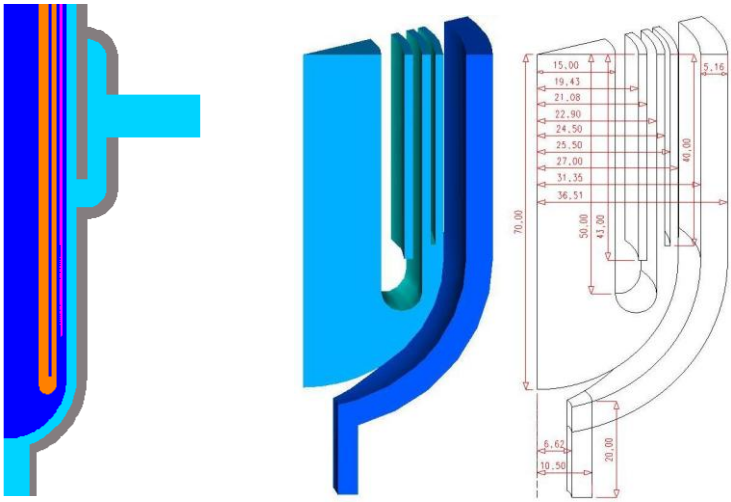

Figure 1: Basic geometry of the pin-cooler, which is axial-symmetrical except for the PbBi inlet. For an easier visualisation, one meter of the cylindrical region has been compressed vertically to one tenth. The small pink region (left picture) is filled with PbBi to detect possible oil leakage.

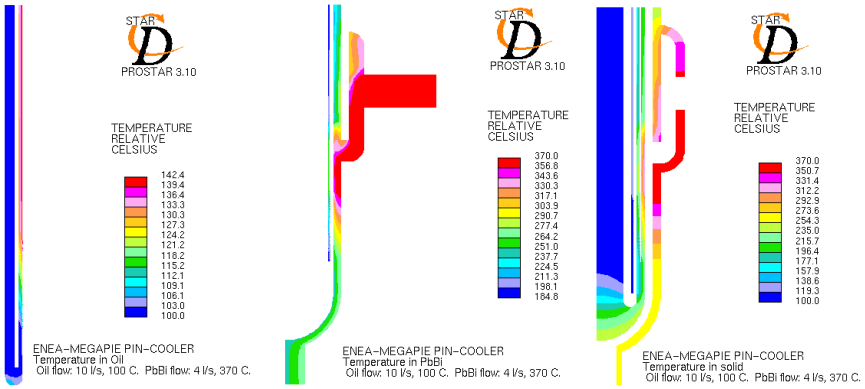

Figure 2: temperature distribution in the first trial pin-cooler geometry.

The temperature field in the solid has been given to ENEA-Bologna for structural calculations. The results, taken from [6], are shown in Figure 3. The maximum Von Mises stress is about 170 Mpa, which has been judged excessive, not allowing a sufficient safety margin. This is one of the reasons that led to abandon the intermediate PbBi channel and to modify the geometry.

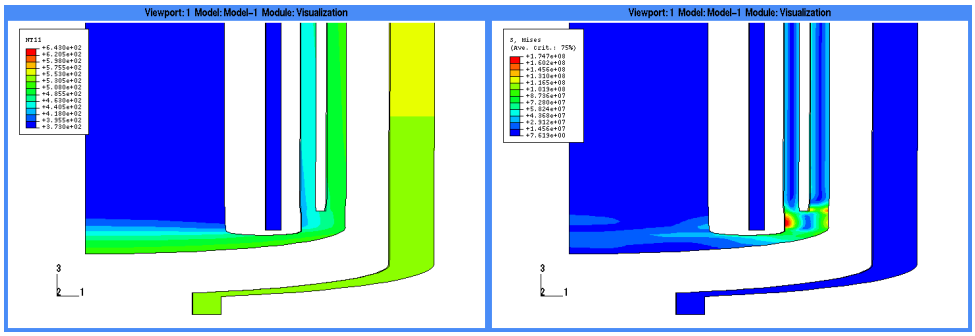

Figure 3: temperature (left) and stress field (right) in the bottom part of the pin-cooler

3 Pin dimensioning

On the basis of the above results, it was decided to limit the wall width between the two fluids to 1.5 mm. The oil used was the Dowtherm A. In spite of its good thermal properties, its resistance to radiation exposure was considered dubious. It was then decided to investigate the possibility of using another oil, namely Diphyl THT oil, which has worse thermal properties but well known behaviour under irradiation. To improve the heat exchange, we have reduced the rising oil channel width. We also looked at the effect of introducing a spiral (30^o over the horizontal plane) in the oil duct, acting as a separator and forcing the flow to rotate while rising. The Reynolds number is therefore increased (by a factor of 2) without increasing the mass flow rate. The simulations are 2D, so that the spiral is simulated indirectly. This point is discussed later in this document. In this case, it is simulated by doubling the mass flow rate while halving the specific heat.

In the simulation matrix, we considered for both oils, two rising channel widths (4.5 and 2.1 mm) with and without spiral. The main flow characteristics are shown in Table 1 while results are shown in Table 2.

	Volume flow rate (l/s)	**Mean velocity (m/s)**	**Inlet temperature (^{o}C)**
Oil (width 4.25 mm)	10 / 12	1.26	100
Oil (width 2.10 mm)	10 / 12	2.58	100
PbBi	4 / 12	0.42	360

Table 1: main flow features

Case	30° separator	Oil	Oil riser width (mm)	Oil outlet temperature (°C)	PbBi outlet temperature (°C)	Pin power (kW)
A1	No	Diphyl THT	4.25	111	327	16.6
A2	Yes	Diphyl THT	4.25	127	277	42.1
A3	No	Dowtherm A	4.25	132	259	51.2
A4	Yes	Dowtherm A	4.25	138	240	60.8
B1	No	Diphyl THT	2.10	121	293	31.9
B2	Yes	Diphyl THT	2.10	140	240	60.8
B3	No	Dowtherm A	2.10	144	224	68.8
B4	Yes	Dowtherm A	2.10	149	209	76.5

Table 2: fluid outlet temperatures and exchanged power for the test matrix

From these preliminary calculations it was clear that it was possible to get the necessary power with the Diphyl THT oil (at least 55 kW including a safety margin), only at the cost of reducing the rising oil channel width and introducing the spiral separator.

4 Spiral analysis

4.1 From 2D to 3D analysis

The presence of the spiral makes the problem non axial-symmetric. From the computational point of view, it obliges to switch from 2D to 3D simulations, which are much more costly. That is why the possibility to simplify the problem back to a 2D flow was investigated.

The problem is to find a 2D flow equivalent to the 3D flow induced by the spiral. In the former analysis, we just modified the mass flow rate and the specific heat in such a way that for a given heat exchange, the outlet temperature is preserved. We should note that the Reynolds number is also preserved. Unfortunately, the Prandtl number is not preserved, and it is not clear how this alters the quality of the analysis. By the way, the simplicity of the procedure makes this method extremely useful as a first approach.

A promising idea has been to modify the fluid properties in order to preserve both the Prandtl and the Reynolds number. It resulted to be impossible without modifying the geometrical fluid properties.

Another idea[1], was to introduce a mass force in the fluid equation in such a way that the flow would get the right swirl. This method has been implemented with promising results. It has nevertheless some drawbacks. First, pressure drops are no more reliable. Second, we implicitly suppose that the flow is almost uniform in the channel created by the spiral, which is far to be obvious. Third, the method tends to be unstable when the angular sector simulated increases and some delicate control mechanism must be implemented.

[1] suggested by Prof. V. Zimont

By the way, these modelling efforts had to be abandoned when we had to face with some technical additional constraints due to the effective pin-cooler construction. In effect, to realise the pin assembly, it is compulsory to let a small gap between the spiral and the external wall, otherwise it would be impossible to assemble the components together. In our case, the gap between the spiral and the wall is 0.6 mm which is far to be negligible in front of the channel width, which is 2.1 mm. In this configuration, only part of the flow is conveyed by the spiral, so creating a flow pattern. It is therefore compulsory to switch to 3D numerical simulations.

4.2 Spiral 3D preliminary study

The problem with 3D geometry is that the mesh number becomes easily huge. To get some feeling about the necessary mesh refinement, we have performed a parametric study. The problem is that the Reynolds number is so low that the requirement on y+ to use wall functions forces us to use very few cells which cannot capture the flow features. We are therefore obliged to use two-layer models, which are again much more costly.

4.2.1 Test case description

The test case is a reduced and simplified pin-cooler with rising oil and down-coming PbBi.

The Oil channel is 2.1 mm wide. On its internal part, a steel spiral of 1.5 mm diameter, is inserted with angle 30^o over the horizontal plane. The spiral pitch is 85 mm. The test case is 6 spiral pitch high. There is no spiral on the top and the bottom pitch. (see Table 3).

Parameter (symbol)	**Value**
Pass (h)	85 mm
Height (H)	510 mm
Spiral diameter (d_S)	1.5 mm
Oil annulus internal diameter (D)	47 mm
Oil annulus width (r_1)	2.1 mm
Steel wall width (r_2)	1.5 mm
PbBi annulus width (r_3)	4.25 mm
Spiral angle over horizontal plane (α)	30^o

Table 3: main geometrical parameters.

Volume flow rates and temperatures are nominal, that is:

- PbBi volume flow rate 4/12 dm^3/s at 360 ^oC inlet temperature.
- Oil volume flow rate: 10/12 dm^3/s at100 ^oC .

The physical properties of the materials are given in appendix.

The pin was tested in the following range of operating conditions:

Power (kW)	10	25	40	55
PbBi flowrate (l/s)	0.05 – 0.4	0.1 – 0.4	0.15 – 0.4	0.25 – 0.4
Coolant flowrate (l/s)	0.1 – 1.0	0.2 – 1.0	0.4 – 1.0	0.6 – 1.0
Coolant inlet temperature (^{o}C)	150 - 300	130 - 250	110 - 200	90 -150

Table 4: range of interest for the pin-cooler characterisation

.

4.2.2 Reynolds and Prandtl numbers

The Reynolds number is given for the volume flow rate of the reference configuration and the channel width is given in Table 3. Only the vertical velocity (2.57 m/s for oil and 0.428 for PbBi) is considered. See table 5.

Fluid	Reynolds Formula	Temp (^{o}C)	Reynolds	Prandtl ($\mu C_p/k$)
LBE	$2 \rho v_z r_3/\mu$	250	19100	$2.58\ 10^{-2}$
		300	20000	$2.19\ 10^{-2}$
		350	22800	$1.91\ 10^{-2}$
Diphyl THT	$2 \rho v_z r_1/\mu$	100	3300	52.8
		160	8200	22.8
		220	13800	14.3
		280	19100	11.2
Dowtherm A	$2 \rho v_z r_1/\mu$	105	11800	13.2
		155	18300	9.3
		205	25600	7.3
		255	34100	6.0

Table 5: Reynolds and Prandtl numbers

Commento [A1]: Come viene definito r3?

Commento [A2]: Come viene definito r1?

4.3 Computational Model

4.3.1 Computational domain and mesh

Due to the presence of the spiral, it is compulsory to make a full 3D simulation. The general mesh structure is shown in Figure 4 and Figure 5. The mesh refining in the external oil side wall is motivated by the use of the two-layers approach on this wall. The mesh has two parameters. The first one is the vertex number which defines the number of nodes along the circumference (which, considering that the basic mesh pattern is a structured rectangle cut along its diagonal to insert the spiral, is equal to the number of cells along the vertical for one pitch). The second one is a refining coefficient (a multiplication factor) for the oil mesh in the radial direction. In Figure 4, they are respectively 36 and 1 and y+ is order one.

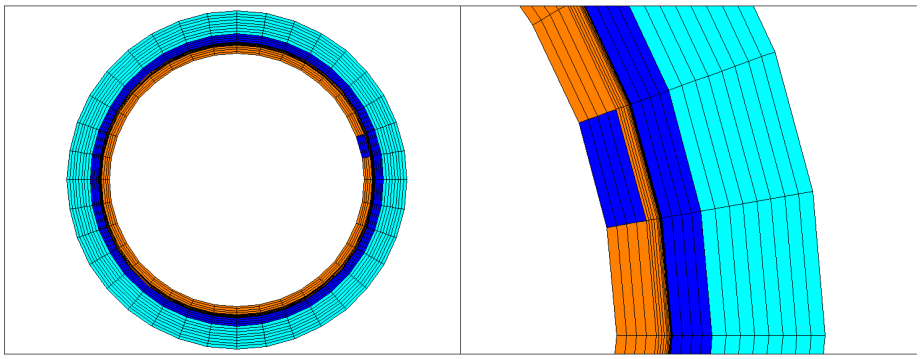

Figure 4: Section of the computational mesh. Pale blue is PbBi, Blue is steel and Orange is oil.

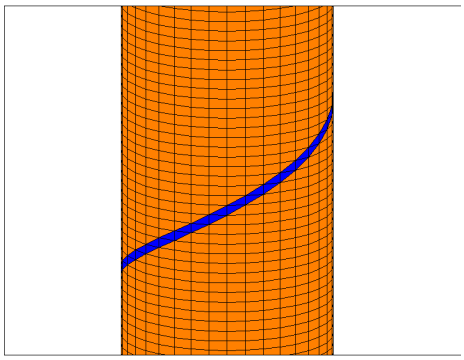

Figure 5: Computational mesh. Zoom on a cylindrical section with the spiral in evidence in blue. The basic mesh pattern is a structured rectangle cut along its diagonal to insert the spiral.

4.3.2 Numerical schemes and turbulence models

QUICK for velocity and temperature, upwind for turbulence equations.

k-ε Chen with two layers on external oil side. Wall functions everywhere else.

4.3.3 Boundary conditions

PbBi inlet on top: downward velocity 0.43 m/s, temperature 360 ^{o}C, Reynolds ≈ 20000.

Oil inlet at bottom: upward velocity 2.6 m/s, temperature 100 ^{o}C, Reynolds 3300.

PbBi outlet at bottom, oil outlet on top and adiabatic walls on domain other boundaries.

4.3.4 Calculation Strategy

Sensibility analysis to mesh refinement.

The azimuth mesh numbers varies from 36 to 90. The oil mesh refinement from 1 to 2.5.

4.4 Results

Main results are summarised in Table .

Case	Azimuth mesh number	Refinement index	Mesh numbers: all, PbBi , Oil	Power [kW]	Convergence (on P)	Pressure drop [kPa]
A1	36	1	246240, 65644, 146592	30.137	$< 10^{-2}$	64.600
A2	36	1.5	320112, 65644, 219888	29.998	$< 10^{-2}$	76.400
A3	36	2	393984, 65644, 293184	30.535	$< 10^{-2}$	96.500
A4	36	2.5	467856, 65644, 366480	34.423	No	179.000
B1	60	1.5	870480, 178560, 599760	30.159	$< 3.10^{-3}$	62.900
B2	60	2.5	1272240, 178560, 999600	30.256	$< 10^{-3}$	82.500
C	72	1.5	1246752, 255744, 859680	30.217	$< 10^{-2}$	60.300
F	90	1.5	1937520, 397440, 1337040	30.315	$2.7*10^{-2}$	58.000

Table 6: list of calculations

The pressure drop seems to be controlled by local effects close to the spiral, which are not accurately taken into account. Moreover, the flow by-passing over the spiral is highly mesh dependent as shown in Table 5 and in Figure 6.
When convergence is reasonable, the exchanged power is remarkably mesh-independent (see figures 8 and 9).

Case	Channelled flow (l/s)	% of total flow	By-passing flow (l/s)	% of total flow
A1	0.33	39	0.51	61
A3	0.15	18	0.69	82

Table 5: Flow split between channelled flow and flow passing over the spiral.

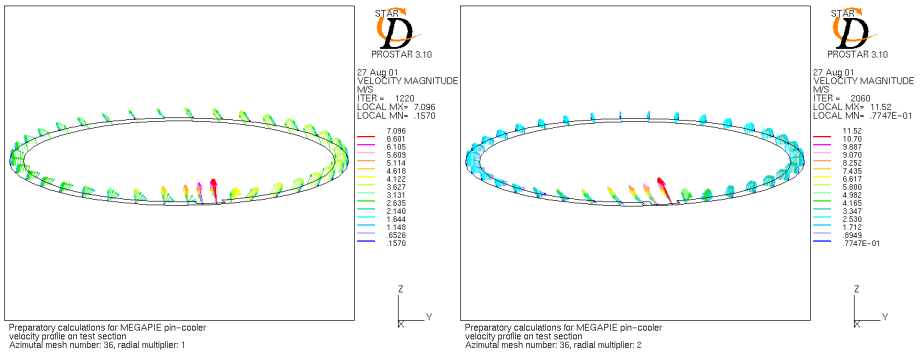

Figure 6: Velocity field on the central test section: case A1 on the left, case A3 on the right. It can be seen that the mesh refinement has the effect of greatly enhancing the flow over the spiral.

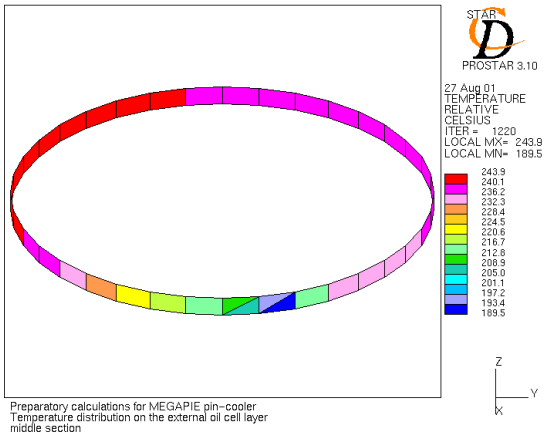

Figure 7: Temperature distribution on the most external oil cell layer on the central test section for case A3. The spiral induces a strong in-homogeneity.

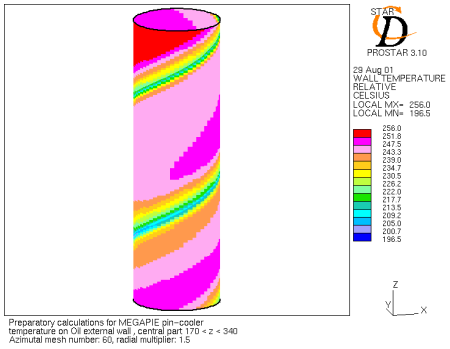

Figure 8: Temperature distribution on the external oil channel wall on the central test section for case B1. The spiral induces variations of about 30°C.

4.5 Conclusions

The introduction of the spiral makes the numerical simulation much more complex. It seems difficult to predict accurately the flow configuration, the pressure drop and the local temperature distribution without describing more accurately the spiral region. The global heat exchange is remarkably independent of the mesh refinement in the range of radial density studied. If the refinement index is at least one, then the mesh density in the other directions is constrained by the necessity of capturing the local flow configuration.

5 Pin-cooler 3D numerical simulation

From the previous considerations, we have decided to simulate the entire pin-cooler with a 3D computational model whose mesh defines accurately the spiral.

5.1 Computational model

5.1.1 Geometry and mesh structure

The geometry has been furnished by ENEA Brasimone [2] in Autocad format, as illustrated in Figure and Figure. As complement, we show in Figure 9 a photo[2] of the pin internal part taken during the pin assembling.

We have made two main simplifications. First, we have not meshed the LBE inlet tube. We just put a lateral LBE inlet of similar section on the cap side, as seen in Figure 10. Second, we have not considered the down-coming oil channel, or the bottom oil flow inversion zone. In this way, the numerical oil inlet is situated at the bottom of the pin and directed upward. These simplifications must be taken into account while interpreting the oil inlet temperature and the oil pressure drop.

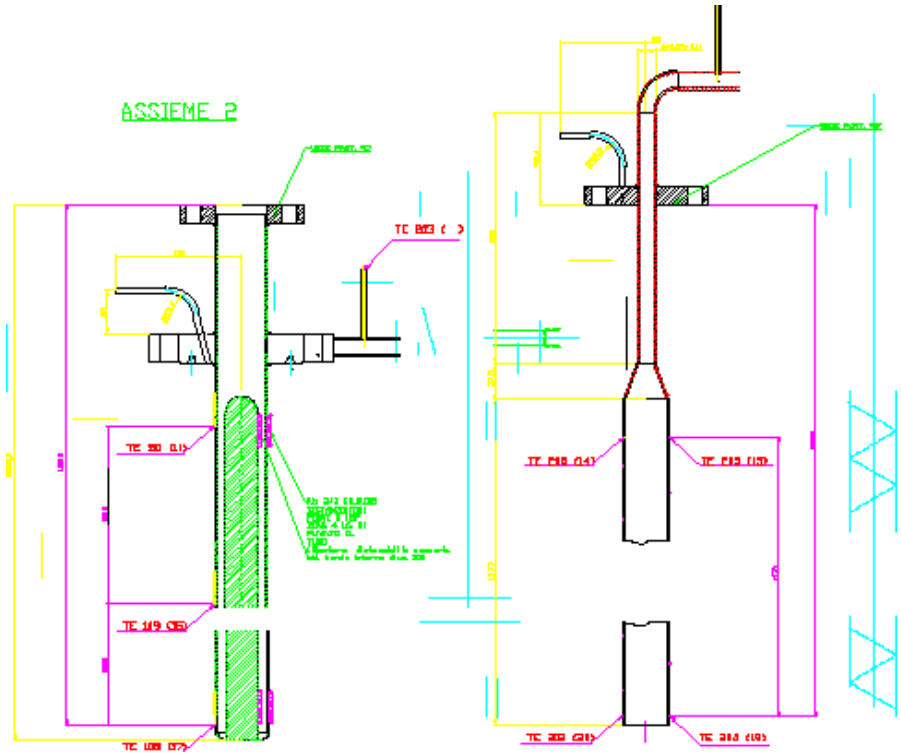

Figure9: pin geometry as from Autocad files, second part. In red are indicated the positions of the thermocouples.

[2] Courtesy of T. Polazzi Enea Brasimone

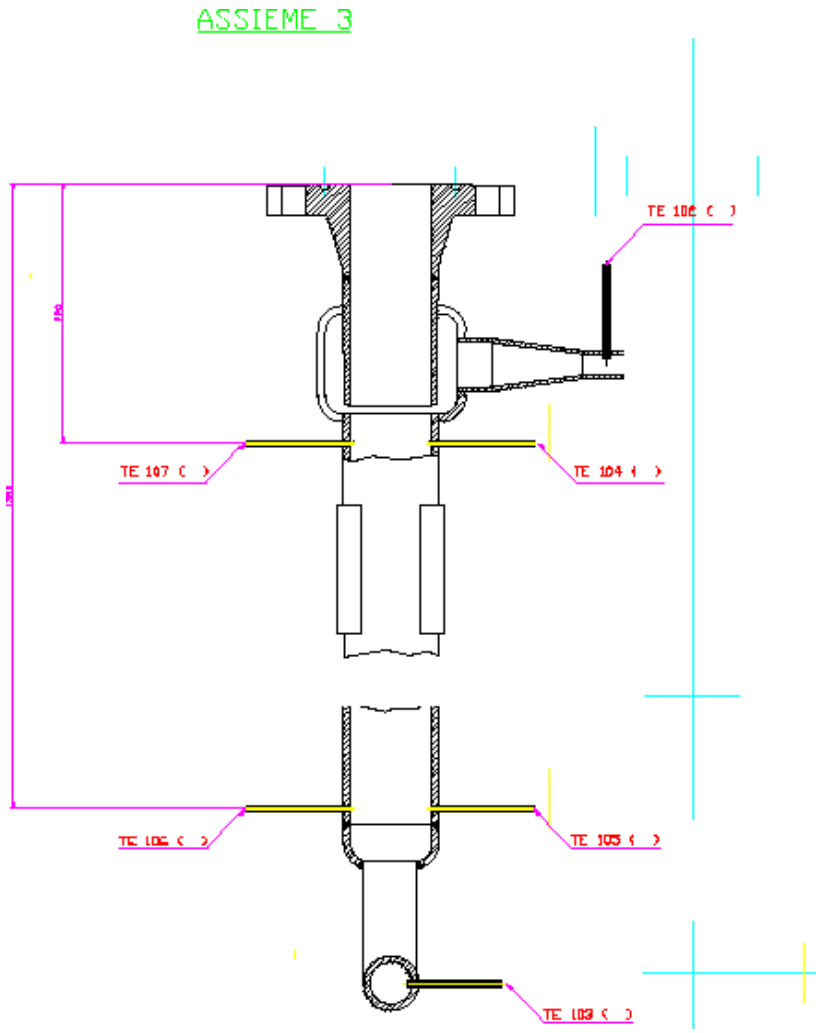

Figure 10: pin geometry as from Autocad files, first part. In red are indicated the positions of the thermocouples.

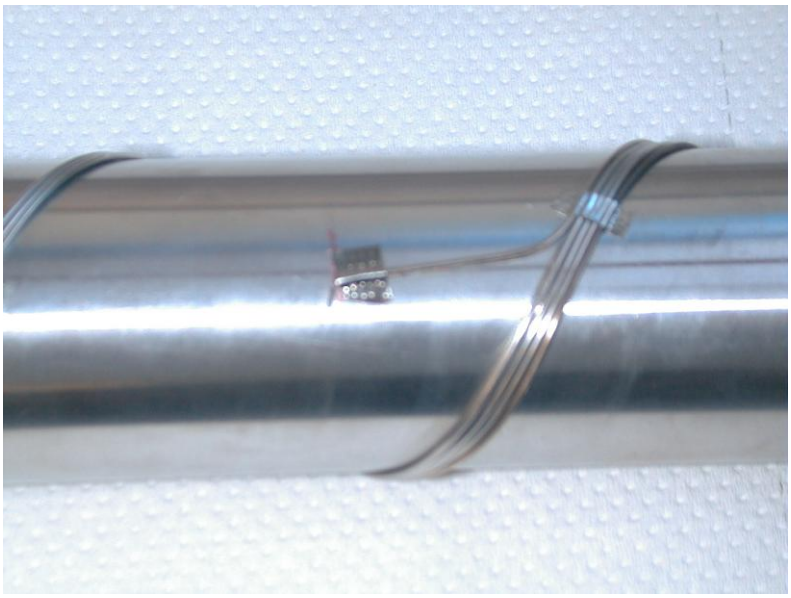

Figure 9: Photo of the pin internal part with the spiral and the thermocouple wires.

The main geometrical parameters are given in Table 6.

Parameter (symbol)	**Value**
Pass (h)	85 mm
Height (H)	510 mm
Spiral diameter (Sd)	1.6 mm
Thermo-couples wire diameter (Wd)	1.0 mm
Number of spiral revolution (N)	15
Oil annulus internal diameter D	47 mm
Oil annulus width (dr1)	2.1 mm
Steel wall width (dr2)	1.5 mm
PbBi annulus width (dr3)	4.25 mm
Spiral angle over horizontal plane (α)	30^o

Table 6: main geometrical characteristics of final computational model

The mesh characteristics are given in Table 7.

Mesh	Cells total	LBE	Oil	Solid	Vertices	Couples
Number	2,666,816	565,389	1,632,320	419,107	2,765,940	28,076

Table 7: main characteristics on the pin-cooler mesh

The mesh characteristics are illustrated in Figure 10 to Figure 15. Note that the mesh is too dense to be visualised at large scale resulting in an all dark image.

From preliminary simulations, it has been seen that a large re-circulation takes place is the would-be stagnant LBE zone in the coaxial cylinder top zone. This re-circulation induced a noticeable asymmetry of the flow temperature. It has then been decided to isolate this LBE region. This is illustrated in Figure 11.

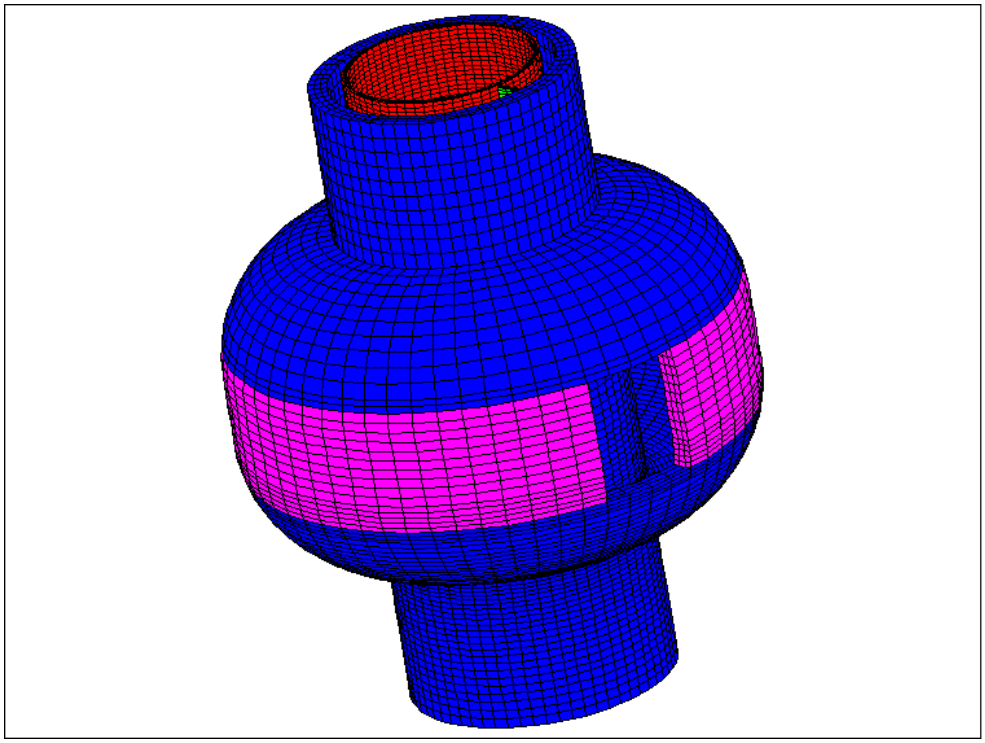

Figure 10: mesh top solid part. The hole in the magenta part is the LBE inlet.

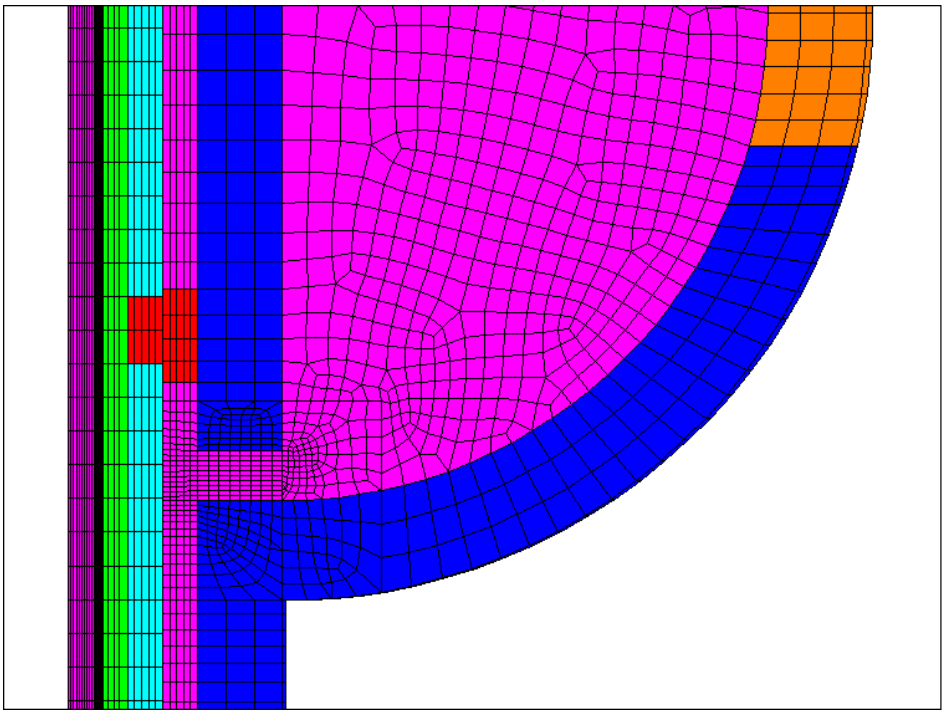

Figure 11: zoom on a section in the LBE inlet zone. From left to right, we have: in violet the oil channel; in green and dark blue, we have the steel walls; in pale blue and lilac, we have the LBE region. In red, we have a steel annulus separating the LBE domain in two unconnected regions. The LBE enters from the right, through the orange region, which extends only on a small angular sector. The left regions are constructed by extrusion following the spiral wire path. The regions on the right have axial-symmetrical meshes. The non-matching connection is done between the two LBE regions.

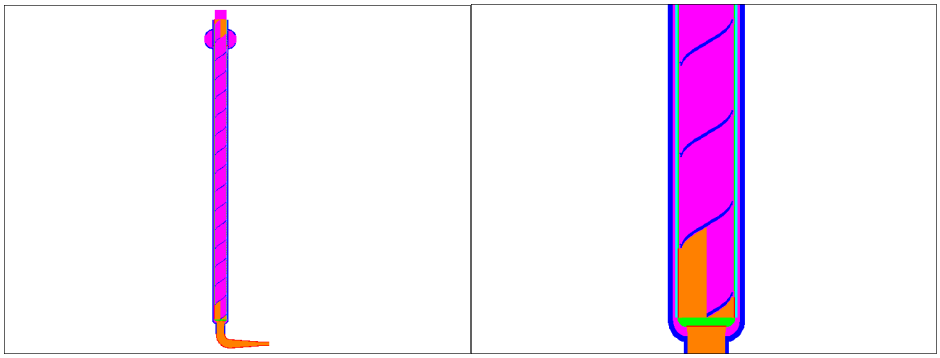

Figure 12: geometry and mesh block structure. At this scale we can not show the mesh because it turns the entire picture black. Only half of the domain is represented to see the internal structure.

We can note the trace of the spiral and a non-conform transition between the orange and violet regions.

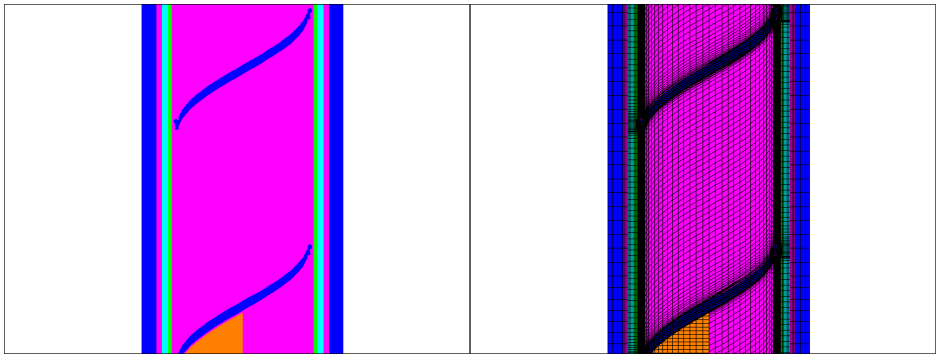

Figure 13: still zooming on the domain, we can see the annular structure and the mesh density.

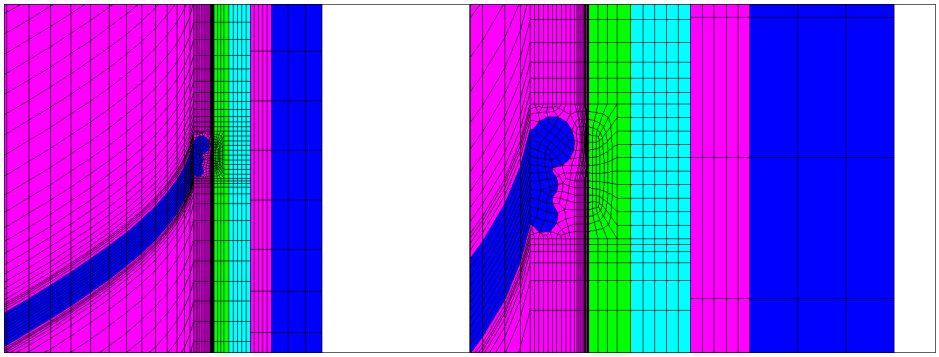

Figure 14: from left to right, we have: spiral and thermocouples wires in blue, oil in violet, solid in green, LBE in pale blue and in violet with a non-matching coupling, external solid in blue.

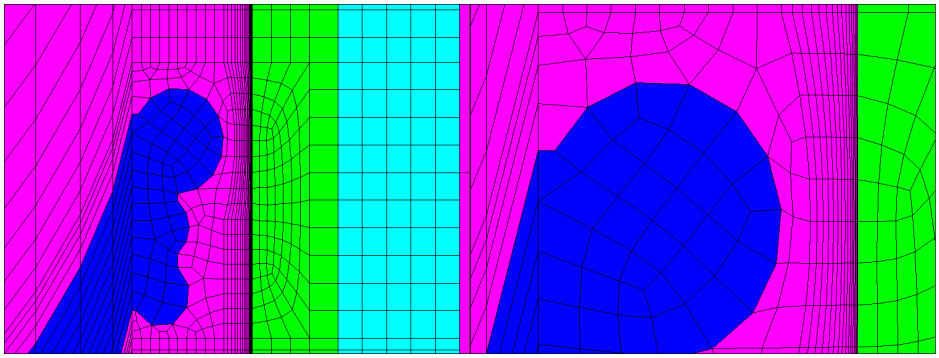

Figure 15: the mesh around the spiral. The difference in the mesh density between LBE and Oil is caused by the difference in the near-wall turbulence models used. A two layers approach is used on the oil side and wall functions are used on the LBE side of the solid.

5.1.2 Numerical schemes and turbulent models

We use the StarCD MARS TVD scheme and the Chen variant of the k-e model. Calculations are stationary and done with the SIMPLE algorithm.

5.1.3 Special features

We have implemented two variants in the turbulence model. First, we have considered a non-standard turbulent Prandtl number Prt, for the LBE. The implementation follows the considerations given in [1] which are particularly suitable for a tube flow. Namely:

$Prt = 0.9 + 182.4/(Pr\ Re^{0.888})$

Where Pr is the Prandtl number and Re is the Reynolds number.

The second variant is a modification of the wall functions of the LBE side. It is motivated by the fact that thermal and dynamic linear sub-layers do not coincide for liquid metals. In StarCD, the y+ value for which one switches from logarithmic to linear profile is the same. We have implemented a separated switch criteria for thermal sub-layer following the method described in CFX.

5.2 Calculation strategy

For the simulations, we chose a significant subset of the experimental test cases to be performed at ENEA Brasimone. The numerical test cases list is given in Table 8, the test cases number referring to the list given in [2].

Case	LBE inlet	Oil inlet	LBE volume	Oil volume	1D power
#5	350	140	1/3	5/6	55
#4	328	161	1/3	5/6	44
#3	305	180	1/3	5/6	33
#2	282	199	1/3	5/6	22
#1	263	220	1/3	5/6	11
#0	243	233	1/3	5/6	2.75
A1	300	150	0.05	0.2	10
A3	226	150	0.4	0.2	10
B1	355	130	0.1	0.3	25
B3	282	130	0.4	0.3	25
C1	373	110	0.15	0.5	40
C3	307	110	0.4	0.5	40
C4	363	200	0.4	0.5	40
C5	328	110	0.15	1.0	40
C8	325	200	0.4	1.0	40
D2	385	150	0.25	0.7	55
D4	356	150	0.4	0.7	55

Table 8: list of simulated cases

The inputs of the numerical simulations are different from the inputs in the experiments. In the numerical simulation, we fix the inlet flow rates and temperatures for both fluids, the exchanged power being a result of the simulation. In the experiment, the thermal power, the flow rate of both fluids and the oil inlet temperature are fixed. In this case, the LBE inlet temperature is a result of the experiment.

In order to have more direct comparison between numerical and experimental results, we have added some additional simulation based on data coming from experimental results. These are listed in Table 9. There was an inconsistency in the experimental data, giving an unbalanced power exchange between the two fluids (case E0). This was caused by an erroneous value given by the LBE flow meter. For this reason, we decided to discard this data and recalculate it from the energy balance (cases E1 and E2).

Case	LBE inlet	Oil inlet	LBE volume	Oil volume	power measured
E0	305.9	137	0.17 (measured)	0.563	31. 24 / 27.43
E1	305.9	137	0.147 (calculated)	0.563	27.43
E2	264.1	136.2	0.155 (calculated)	0.556	21.59

Table 9: calculation matrix from direct experimental data

5.3 Results

5.3.1 Main results

Main results are given in Table 10 to Table 12. A comparison between numerical and experimental results is given in Table 13. Results are discussed in section 5.4

Termocouple	Height (mm)	#0	#1	#2	#3	#4	#5
		LBE Temperature (C)					
T102 (LBE inlet)	1270	243	263	282	305	328	350
T104	1194	242.6	261	278.3	298.8	319.6	340.5
T107	1194	242.5	260.9	278	298.1	318.5	338.1
T105	24	237.3	238.6	235	234.6	234.1	234.3
T106	24	237.2	238	233.8	232.7	231.8	231.5
T103 (LBE outlet)	-111	237.3	238.5	234.9	234.5	234.1	234
		Oil temperature (C)					
T205	1194	235	228.2	214.4	202.7	188.8	172.23
T206	1194	235	228.3	214.6	202.9	189.14	172.57
T204	24	233	220	199	179.99	160.98	139.98
T202	24	233	220	199.03	180.04	161.03	140.02
		Wall temperature LBE side (C)					
T110	1194	241.3	255.9	268.4	283.7	299.3	315
T109	609	237.9	240.8	238.9	240.7	242.2	244
T108	24	236.2	233.7	225.6	220.6	215.9	212.3
				I/O (C)			
LBE inlet T	1270	243	263	282	305	328	350
Oil inlet T	0	233	220	199	180	161	140
LBE outlet T	-111	237.21	238.06	234.02	233.19	232.36	232.11
Oil outlet T	1402	235.23	229.38	216.64	205.95	193.21	177.37
Power (kW)		2.95	12.65	24.24	36.19	48.04	59.03
		Pressure (kPa)					
dP LBE	1382	108.9	108.9	109.0	109.0	109.3	109.1
dP Oil	1402	126.5	128.2	131.7	134.8	138.5	143.0

Table 10: main results first series

Termocouple	Height (mm)	A1	A3	B1	B3	C1	C3
		LBE Temperature (C)					
T102 (LBE inlet)	1270	300	226	355	282	373	307
T104	1194	279.8	225.0	334.9	279.1	352.3	301.7
T107	1194	266.1	224.1	325	277.3	347.6	299.9
T105	24	165.5	208.4	185.6	237.3	191.9	235.4
T106	24	165.2	207.7	185.6	235.3	189.7	232.9
T103 (LBE outlet)	-111	164.4	208.4	183.6	237	189.4	235.3
		Oil temperature (C)					
T205	1194	179.7	176.2	166.0	173.0	146.1	151.2
T206	1194	170.1	176.3	166.7	173.5	146.8	151.9
T204	24	150.0	150.0	130.0	130.1	110.0	110.0
T202	24	150.0	150.0	130.0	130.0	110.0	110.0
		Wall temperature LBE side (C)					
T110	1194	254.5	221.5	307.0	269.3	318.7	285.8
T109	609	189.4	210.2	218.9	240.4	220.9	239.6
T108	24	163.3	202.3	178.1	223.9	177.1	216.8
		Inlet/Outlet (C)					
LBE inlet T	1270	300	226	355.0	282.0	373.0	307.0
Oil inlet T	0	150	150	130.0	130.0	110.0	110.0
LBE outlet T	-111	164.3	207.72	182.8	236.0	187.9	233.8
Oil outlet T	1402	176.7	179.15	175.1	178.7	154.5	157.3
Power (kW)		**10.22**	**11.19**	**25.81**	**27.93**	**41.52**	**44.3**
		Pressure (kPa)					
dP LBE	1382	140.9	95.4	138.0	95.2	134.3	95.4
dP Oil	1402	27.1	27.1	40.7	39.3	81.0	78.3

LBE flow (l/s)		0.05	0.4	0.1	0.4	0.15	0.4
Oil flow (l/s)		0.2	0.2	0.3	0.3	0.5	0.5
Section vertical velocity (m/s)		0.657	0.661	0.991	0.997		
Section horiziontal velocity (m/s)		0.425	0.435	0.672	0.688		
Mean angle		57.1	56.6	55.9	55.4		

Table 11: main results second series

Termocouple	Height (mm)	C4	C5	C8	D2	D4	E0
		LBE Temperature (C)					
T102 (LBE inlet)	1270	363	328	325	385	356	305.5
T104	1194	357.6	306.2	319.1	368.9	348.2	293.3
T107	1194	357.1	302.6	318.3	365.6	345.8	288.3
T105	24	290.1	154.2	255.3	234.8	257.9	188.5
T106	24	287.9	152.4	255.3	231.4	254.7	186.4
T103 (LBE outlet)	-111	290.4	152.4	255.1	233.7	257.9	187.0
		Oil temperature (C)					
T205	1194	239.1	127.4	218.8	185.6	188.9	161.0
T206	1194	239.4	127.7	219.0	186.1	189.3	161.5
T204	24	200.0	110.0	200.0	150.0	150.0	137.0
T202	24	200.1	110.0	200.0	150.0	150.0	137.0
		Wall temperature LBE side (C)					
T110	1194	343.7	269.7	302.6	337.9	326.3	268.9
T109	609	296.4	175.8	258.6	251.0	263.3	205.4
T108	24	271.7	142.7	239.9	214.1	234.4	176.9
		Inlet/Outlet					
LBE inlet T	1270	363.0	328.0	325.0	385	256	305.5
Oil inlet T	0	200.0	110.0	200.0	150	150	137
LBE outlet T	-111	288.5	151.3	254.0	231.9	255.8	186.1
Oil outlet T	1402	244.0	131.9	221.5	191.8	194.2	165.8
Power (kW)		**44.69**	**39.83**	**42.87**	**56.80**	**60.17**	**30.61**
		Pressure (kPa)					
dP LBE	1382	94.9	135.1	95.2	122.6	95.3	132.8
dP Oil	1402	58.4	228.6	176.6	105.9	105.2	84.0

LBE flow (l/s)		0.4	0.15	0.4	0.25	0.4	0.17
Oil flow (l/s)		0.5	1	1	0.7	0.7	0.56
Section vertical velocity			3.29	3.29	2.32	2.32	1.85
Section horiziontal velocity			2.49	2.73	1.84	1.86	1.37
Mean angle			52.87	50.31	51.5	51.3	53.4

Table 12: main results third series

Termocouple	Height (mm)	E1	E1 numerical	E2	E2
		LBE Temperature (^{o}C)			
T102 (LBE inlet)	1270	305.9	305.9	264.1	264.1
T104	1194	280.4	292.4	243.1	254.5
T107	1194	307.2	283.6	265.5	249.6
T105	24	188.8	181.6	177.9	173.7
T106	24	174.1	179.7	165.4	172.0
T103 (LBE outlet)	-111	182.8	180.0	172.7	172.6
		Oil Temperature (^{o}C)			
T205	1194	162.0	159.5	156.6	154.0
T206	1194	162.1	160.0	156.3	154.4
T204	24	141.2	137.0	140.0	136.2
T202	24	138.8	137.0	137.6	136.2
		Wall temperature LBE side (^{o}C)			
T110	1194	288.2	263.3	250.8	235.1
T109	609	206.1	200.2	190.5	187.2
T108	24	167.5	171.4	160.7	165.2
		Inlet / Outlet temperature (^{o}C)			
LBE inlet T	1270	305.9		264.1	
Oil inlet T	0 / 1400	137.0		136.2	
LBE outlet T	-111	182.8	179.1	172.7	171.9
Oil outlet T	1402	163.5	164.4	157.1	157.7
Power (kW)		**27.43**	**28.32**	**21.59**	**21.75**
		Pressure (kPa)			
dP LBE	1382	99.9	134.9	101.7	134.6
dP Oil	1402	189.9	81.7	191.7	82.1

LBE flow (l/s)		0.147		0.155	
Oil flow (l/s)		0.563		0.556	
Section vertical velocity			1.79		1.77
Section horizontal velocity			1.33		1.30
Mean angle			53.5		53.8

Table 13: Comparison between numerical and experimental results

.

5.3.2 Flow angle and Reynolds number

The oil flow mean inclination at the half height of the pin is shown in Table 14 for case #1. We can note that the mean flow angle is much higher than the spiral angle, as illustrated in Figure 16. Therefore, the mean velocity module is also quite less than expected and the mean path length is not doubled but only increased by a factor of 1.2 to 1.3, as shown in Table 15.

The Oil flow mean inclination being not known a priori, the Reynolds number is also not known and is a result of the simulation. It is given in Table 16 as well as other physical characteristics of the fluid and is taken in a section situated in the middle of the pin.

Oil vertical section of 85 mm height (1 pitch)	Area	173.85 mm^2
	Volume flow rate	0.389 l/s
	Volume averaged horizontal velocity	2.24 m/s
Oil horizontal middle section	Area	315.5 mm^2
	Volume flow rate	0.867 l/s
	Volume averaged vertical velocity	2.73 m/s
Velocity Module	Mean	3.5 m/s
Mean Flow angle	Volume averaged	50.6°

Table 14: data for oil flow orientation case #1

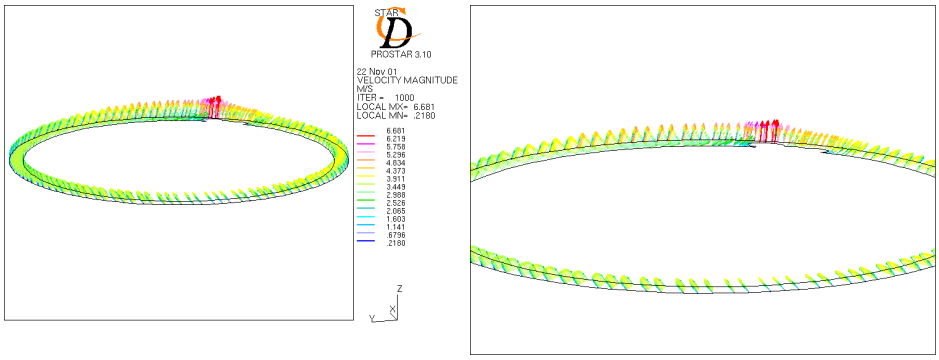

Figure 16: Flow field of the oil in the half height section of the pin for case 1.5. We can see that the flow is not homogeneous and that the mean angle is higher than the spiral angle (30 degrees).

Case	Oil section mean	Oil section mean	Mean oil flow	Mean length (or velocity)
#1	2.73	2.24	50.6	1.29
#4	2.75	2.24	50.8	1.29
A1	0.657	0.425	57.1	1.19
A3	0.661	0.435	56.6	1.20
B1	0.991	0.672	55.9	1.21
B3	0.997	0.688	55.4	1.21
C5	3.29	2.49	52.9	1.25
C8	3.29	2.73	50.3	1.30
D2	2.32	1.84	51.5	1.28
D4	2.32	1.86	51.3	1.28
E0	1.85	1.37	53.4	1.25
E1	1.79	1.33	53.5	1.24
E2	1.77	1.30	53.8	1.24

Table 15: mean flow angle for some test cases and equivalent length factor (ratio between the flow path length and the pin height.

Case	Oil section mean	Section mean	Section mean	Section mean	Reynolds
#1	223.7	3.58	869.3	$0.672\ 10^{-3}$	19500
#4	172.7	3.59	902.2	$0.101\ 10^{-2}$	13500
A1	156.3	0.793	912.7	$0.124\ 10^{-2}$	2450
A3	164.7	0.802	907.3	$0.112\ 10^{-2}$	2730
B1	144.3	1.22	920.4	$0.149\ 10^{-2}$	3200
B3	152.8	1.23	915.0	$0.132\ 10^{-2}$	3600
C5	116.3	4.18	938.5	$0.233\ 10^{-2}$	7000
C8	208.4	4.34	879.2	$0.737\ 10^{-3}$	21500
D2	165.0	3.01	907.1	$0.111\ 10^{-2}$	10300
D4	168.2	3.01	905.1	$0.107\ 10^{-2}$	10700
E0	146.9	2.33	918.8	$0.142\ 10^{-2}$	6300
E1	145.9	2.26	919.4	$0.144\ 10^{-2}$	6100
E2	143.6	2.23	920.9	$0.150\ 10^{-2}$	5750

Table 16: physical characteristics of the oil flow in a section in the middle of the pin and corresponding Reynolds number.

5.3.3 Effects of the modifications on the turbulence modelling

In Table 17, we show the effects of the special treatment of the LBE wall functions (WF) and of the modified turbulent Prandtl number (Prt).

Case	#0	#0a	#1	#1a	#5	#5a	#5b
Modified	Yes	No	Yes	No	Yes	Yes	No
Modified Prt	Yes	Yes	Yes	Yes	Yes	No	No
Power (kW)	2.95	2.66	12.65	11.37	59.03	60.35	57.6

Table 17: effects of the special treatment of the LBE wall functions (WF) and of the modified turbulent Prandtl number (Prt)

In the cases under study, the modified wall functions implementation causes an increase of the heat exchange by 5 to 10%, while the modified turbulent Prandtl number causes a decrease of the heat exchange by 2.5%.

5.4 Discussion

Results show a slightly better behaviour than expected from mono-dimensional calculations. The heat exchange improvement is the result of a balance between a mean velocity smaller than expected and a greater turbulence generation caused by the flow by-passing the spiral wire. This balance is very difficult to estimate a priori with 1D calculations, making the 3D simulation compulsory.

The agreement between numerical and experimental values is very good on the overall heat exchange with a power discrepancy about 3.5% for case E1 and less than 1% for case E2. It seems that the physical phenomenology has been captured.

The numerical results agree quite well with the “oil” thermocouples. The spiral induces a good uniformity of the oil flow all around the circumference. From the LBE side, the situation is quite different. The numerical analysis predicts a higher temperature on the inlet side (T104) than on the opposite side (T107) with a difference rapidly decreasing downward (T105 and T106). Experiments give a smaller temperature on the inlet side with more marked difference which survives down to pin bottom The LBE temperature is therefore quite non-symmetric. It is difficult to understand this behaviour. It may be that the separators, which are not simulated, are placed close to the thermocouples on the inlet side and perturb the flow. It may also be that the flow is not uniform due to small temperature induced deformations in critical parts. The most critical part seems to be the 2mm high circular gap, which the LBE enter the coaxial channel through.

The wall temperature given by the thermocouples is higher than the numerical wall temperature. This is congruent with the previous point. Moreover, according the to the experimental staff, the “wall” thermocouples, being attached to the wall and not incorporated in it, do not exactly measure the wall temperature but some kind of mean temperature very close to the wall which is a little higher.

The pressure losses do not match experimental data. The LBE pressure drop is not a priori subject to a large numerical error, being quite simple to simulate. The discrepancy can be congruent with the local LBE temperature one, indicating that the pin has withstood unacceptable deformations, either at building time or when put in charge. The preliminary calculations showed that the oil pressure drop is extremely sensitive to meshing and/or geometric perturbations, due to, say, temperature induced deformations, while the heat exchange is not. That is exactly what is observed.. The hypothesis of mechanical deformation was effectively demonstrated after dismantling the component. Such deformation was due to erroneous construction procedure and was located in proximity of the LBE inlet gap; it generated also the circumferential temperature differences. Moreover, the pressure drop along the oil side could be not reproducible and give other values for other pin-coolers. As they are supposed to be put in parallel in the Megapie apparatus, this could result in a strong in-homogeneity of fluid flow rates.

6 Conclusions

By means of the CFD tools, we have contributed to the dimensioning of a Pin-Cooler for the Megapie experiment. We have given indications for the choice of the secondary coolant and raised the potential problems of excessive stress, which has been solved before the actual pin construction. Due to the complexity of the geometry, mainly induced by the insertion of a spiral wire partially obstructing the secondary coolant channel, we have performed a full 3D numerical analysis of the experimental pin. The simulation results on the exchanged power are within 4% error with the experiment. This is a very good indication that the local behaviour of the flow is very similar to the one simulated. The global power exchanged is well reproduced, confirming that it is only slightly dependent on small geometrical variations and that the physics of the experiment is captured. The error on local temperatures is higher and may be the indication that the pin-cooler has sustained some deformation in the experiment. The oil side pressure losses do not agree with experimental data, being extremely sensitive to geometric perturbations due to, say, temperature induced deformations. This can be a serious problem in the perspective of having 12 pin-cooler in parallel with a uniform repartition of the flows.

7 References

[1] M. Jischa, H.B. Rieke, Modeling assumptions for turbulent heat transfer

[2] T. Polazzi, Progetto di prova: prova Megapie "Cooling Pin", ENEA Progetto ADS Report GS2-TR-00003 December 2001

[3] S. Cevolani, “Review of the Liquid Lead-Bismuth Alloy Physical Properties”, ENEA Technical Report DT.SBD.00004, ENEA, April 1998.

[4] STAR-CD, Version 3.15 Manual, Computational Dynamics, London, 2001.

[5] I-DEAS Master series, Reference Manual, 1996, SDRC (Structural Dynamics Research Corporation).

[6] A. Zucchini, ENEA-Bologna, personal communication

[7] P. Agostini, ENEA-Brasimone, personal communications

[8] N.I.Tak, X. Cheng, “Numerical Design of the Active Part of the MEGAPIE target”, FZKA 6611, FZKA, Karlsruhe, 2001.

Appendix A. Physical properties tables

The PbBi, Diphyl THT and Dowtherm A oil properties are given in Table 18, Table 19 and Table 20. They are numerically approximated by best fit polynomial functions in Table 21, Table 22 and Table 23.

Temperature (^oC)	Density ($kg.m^{-3}$)	Thermal conductivity ($W\ m^{-1}K^{-1}$)	Dynamic viscosity ($kg\ m^{-1}\ s^{-1}$)	Heat Capacity ($J\ kg^{-1}K^{-1}$)	Prandtl Number (-)
130	10558	8.96	$2.52 \cdot 10^{-3}$	146.5	$4.66 \cdot 10^{-2}$
150	10531	9.11	$2.43 \cdot 10^{-3}$	146.5	$4.10 \cdot 10^{-2}$
175	10496	9.41	$2.31 \cdot 10^{-3}$	146.5	$3.57 \cdot 10^{-2}$
200	10462	9.72	$2.19 \cdot 10^{-3}$	146.5	$3.16 \cdot 10^{-2}$
225	10428	10.0	$2.09 \cdot 10^{-3}$	146.5	$2.84 \cdot 10^{-2}$
250	10393	10.3	$1.98 \cdot 10^{-3}$	146.5	$2.58 \cdot 10^{-2}$
275	10359	10.6	$1.89 \cdot 10^{-3}$	146.5	$2.37 \cdot 10^{-2}$
300	10325	10.9	$1.80 \cdot 10^{-3}$	146.5	$2.19 \cdot 10^{-2}$
325	10290	11.3	$1.71 \cdot 10^{-3}$	146.5	$2.04 \cdot 10^{-2}$
350	10256	11.6	$1.64 \cdot 10^{-3}$	146.5	$1.91 \cdot 10^{-2}$
375	10221	11.9	$1.56 \cdot 10^{-3}$	146.5	$1.79 \cdot 10^{-2}$
400	10187	12.2	$1.50 \cdot 10^{-3}$	146.5	$1.69 \cdot 10^{-2}$
425	10153	12.5	$1.44 \cdot 10^{-3}$	146.5	$1.60 \cdot 10^{-2}$
450	10118	12.8	$1.38 \cdot 10^{-3}$	146.5	$1.52 \cdot 10^{-2}$
475	10084	13.1	$1.33 \cdot 10^{-3}$	146.5	$1.45 \cdot 10^{-2}$
500	10050	13.4	$1.29 \cdot 10^{-3}$	146.5	$1.38 \cdot 10^{-2}$
525	10015	13.7	$1.25 \cdot 10^{-3}$	146.5	$1.32 \cdot 10^{-2}$
550	9981	14.0	$1.22 \cdot 10^{-3}$	146.5	$1.27 \cdot 10^{-2}$
575	9946	14.3	$1.19 \cdot 10^{-3}$	146.5	$1.22 \cdot 10^{-2}$
600	9912	14.6	$1.17 \cdot 10^{-3}$	146.5	$1.17 \cdot 10^{-2}$

Table 18: Lead-Bismuth physical properties as given by the selected relationships

Temperature (^oC)	Vapour pressure (bar)	Dynamic viscosity (mPa.s)	Density (kg/m^3)	Specific heat (kJ/kgK)	Thermal conductivity (W/mK)
100		3.12	949	1.810	0.107
115		2.32	939	1.860	0.107
130		1.81	930	1.911	0.106
145		1.45	920	1.962	0.106
160	0.003	1.20	910	2.014	0.106
175	0.006	1.02	901	2.065	0.105
190	0.011	0.88	891	2.117	0.105
205	0.019	0.77	881	2.169	0.104
220	0.032	0.68	872	2.222	0.104
235	0.053	0.62	862	2.275	0.104
250	0.083	0.56	852	2.328	0.103
265	0.128	0.51	843	2.381	0.103
280	0.190	0.47	833	2.434	0.102
295	0.276	0.44	823	2.488	0.102
310	0.392	0.41	814	2.542	0.102
325	0.546	0.38	804	2.597	0.101
340	0.745	0.36	794	2.651	0.101
355	0.999	0.34	785	2.706	0.101

Table 19: Diphyl THT oil physical properties

Temperature (^oC)	Vapour pressure (bar)	Dynamic viscosity (mPa.s)	Specific heat (kJ/kgK)	Thermal conductivity (W/mK)	Density (kg/m^3)
65	0.00	1.58	1.701	0.1315	1023.7
105	0.01	0.91	1.814	0.1251	990.7
155	0.06	0.56	1.954	0.1171	947.8
205	0.28	0.38	2.093	0.1091	902.5
255	0.97	0.27	2.231	0.1011	854.0
305	2.60	0.20	2.373	0.0931	801.3
355	5.80	0.16	2.527	0.0851	742.3
405	11.32	0.12	2.725	0.0771	672.5

Table 20: Dowtherm A oil physical properties

Parameter (symbol)[units]	Formula (temperature in K)	Value at 300 C	Value at 400 C	Value at 500 C
Density (ρ_w) [kg/m^3]	11112. – 1.37 T	10327	10190	10053
Dynamic viscosity (μ) [kg/m/s]	$4.71\ 10^{-9}\ T^2 – 8.92\ 10^{-6} T + 5.37\ 10^{-3}$	$1.81\ 10^{-3}$	$1.5\ 10^{-3}$	$1.29\ 10^{-3}$
Surface tension (σ) [N/m]	$0.473 – 1.03\ 10^{-4} T$	0.414	0.404	0.395
Thermal conductivity (k) [W/m/K]	7.26 + 0.0123 (T-273)	11.0	12.9	15.4
Specific heat (C_p) [J/kg/K]	146.5	146.5	146.5	146.5

Table 21: physical properties of the PbBi eutectic

Parameter (symbol)[units]	Formula (temperature in ^{0}C, except for viscosity in K)
Density (ρ) [kg/m^3]	949. – 29/45 * (T-100)
Dynamic viscosity(μ) [kg/m/s]	$1.5\ 10^{-2}.–2.10\ 10^{-4}\ T+1.17\ 10^{-6}\ T^2 –2.94\ 10^{-9}\ T^3+ 2.75\ 10^{-12} T^4$
Thermal conductivity(k) [W/m/K]	$0.107 – 2.7\ 10^{-5}$(T-100)
Specific heat(C_p) [J/kg/K]	1810+3.4*(T-100)
Specific heat(C_p^*) [J/kg/K]	$1810+3.4/2\ *(T-100)^2/(T+273)$

Table 22: Diphyl THT approximation by best fit of physical properties C_p^* is the effective non standard implementation of variable specific heat in StarCD.

Parameter (symbol)[units]	Formula (temperature in K)
Density (ρ) [kg/m^3]	990.7 – 0.858 (T-378)
Dynamic viscosity (μ) [kg/m/s]	$3.08\ 10^{-3} – 2.98\ 10^{-5}\ T + 8.73\ 10^{-8}\ T^2$
Thermal conductivity (k) [W/m/K]	$0.1288 – 1.4\ 10^{-4}$(T-355.8)
Specific heat (C_p) [J/kg/K]	1814 + 2.8(T-378)
Specific heat (C_p^*) [J/kg/K]	$1814 + 2.8/2\ *(T-378)^2/T$

Table 23: Dowtherm A oil approximation by best fit of physical properties C_p^* is the effective non standard implementation of variable specific heat in StarCD.